Current Applied Physics 19 (2019) 1040–1045

Contents lists available at ScienceDirect

Current Applied Physics

journal homepage: www.elsevier.com/locate/cap

Experimental evidence of breakdown strength and its effect on energy-storage performance in normal and relaxor ferroelectric films

Minh D. Nguyen[a,b,c,*], Chi T.Q. Nguyen[d,e], Hung N. Vu[d], Guus Rijnders[c]

[a] Division of Computational Mechatronics, Institute for Computational Science, Ton Duc Thang University, Ho Chi Minh City, Viet Nam
[b] Faculty of Electrical & Electronics Engineering, Ton Duc Thang University, Ho Chi Minh City, Viet Nam
[c] MESA + Institute for Nanotechnology, University of Twente, P.O. Box 217, 7500AE, Enschede, the Netherlands
[d] International Training Institute for Materials Science (ITIMS), Hanoi University of Science and Technology, 1 Dai Co Viet Road, Hanoi, Viet Nam
[e] Vietnam National University of Forestry, Xuan Mai Town, Chuong My District, Hanoi, Viet Nam

ARTICLE INFO

Keywords:
Polar nano-regions
Relaxor ferroelectric
Breakdown strength
Energy-storage density
Energy efficiency

ABSTRACT

Normal-ferroelectric $Pb(Zr_{0.52}Ti_{0.48})O_3$ (PZT) and relaxor-ferroelectric $Pb_{0.9}La_{0.1}(Zr_{0.52}Ti_{0.48})O_3$ (PLZT) thin-films are deposited on $SrRuO_3$-covered $SrTiO_3$/Si substrates. An ultrahigh recoverable energy-storage density (U_{reco}) of 68.2 J/cm^3 and energy efficiency (η) of 80.4% are achieved in the PLZT thin-films under a large breakdown strength (E_{BD}) of 3600 kV/cm. These values are much lower in the PZT thin-films (U_{reco} of 10.3 J/cm^3 and η of 62.4% at E_{BD} of 1000 kV/cm). In addition, the remanent polarization (P_r) and dielectric-constant are also investigated to evaluate the breakdown strength in thin-films. Polar nano-regions (PNRs) are created in the PLZT thin-films to enable relaxor behavior and lead to slim polarization loops along with very small P_r. The excellent operating temperature of energy-storage performance and also the breakdown strength obtained in the PLZT thin-films are mainly ascribed to the presence of PNRs. Moreover, both PZT and PLZT thin-films exhibit superior performance up to 10^{10} times of charge-discharge cycling.

1. Introduction

Pulse power energy-storage systems have important applications in many fields, from electrical power grids and transportation systems to medical devices, such as artificial pacemakers and defibrillators [1–5]. In these applications, there are various types of pulsed loads that have a high instantaneous power requirement in a very short duration (typically ranging from microseconds to milliseconds) [6]. Dielectric capacitors, which have high energy-storage density and fast charge-discharge rates, have been widely used in these power systems.

The energy-storage density of a dielectric capacitor, such as normal ferroelectric, relaxor ferroelectric and antiferroelectric materials, is governed by the applied electric field (E) and is determined by integrating the area under the polarization hysteresis (P-E) loops [7–9]. The 'charge' energy stored per unit volume (U_{store}), recoverable 'discharge' energy-storage density (U_{reco}) and energy-storage efficiency (η) can be calculated by:

$$U_{store} = \int_0^{P_{max}} EdP \quad (1)$$

$$U_{reco} = \int_{P_r}^{P_{max}} EdP \quad (2)$$

$$\eta(\%) = 100 \times U_{reco}/U_{store} \quad (3)$$

where P_r and P_{max} are the remanent polarization and maximum polarization, respectively. The maximum applied electric field (E_{max}) must be equal to or less than the critical electric-field breakdown strength (E_{BD}), just below the electric field where the capacitor is broken completely [8].

According to Eqs. (1) and (2), a large E_{BD} guarantees a high energy-storage density. In general, small and homogeneous grain sizes, as well as the densification of the capacitor structures, are beneficial to obtaining a high E_{BD} value [8–13]. Yang et al. reported that the E_{BD} of (1-x)$SrTiO_3$-x($0.93Bi_{0.5}Na_{0.5}TiO_3$-$0.07Ba_{0.94}La_{0.04}Zr_{0.02}Ti_{0.98}O_3$) ($x$ = 0.0–0.5) ceramics decreases from ~325 to ~170 kV/cm with increasing average grain size from 1.09 (x = 0.0) to 4.86 μm (x = 0.5) [9]. The densification was also found to increase the E_{BD} in (1-x)$BaTiO_3$-xBi($Mg_{2/3}Ni_{1/3}$)O_3 (BT-BMN) ceramics, in which the BMN content (x = 0.05–0.2) could promote the densification and then the breakdown strength of the ceramics [10]. In the thin-film structures,

* Corresponding author. Division of Computational Mechatronics, Institute for Computational Science, Ton Duc Thang University, Ho Chi Minh City, Viet Nam.
E-mail address: nguyenducminh@tdtu.edu.vn (M.D. Nguyen).

https://doi.org/10.1016/j.cap.2019.06.005
Received 27 April 2019; Received in revised form 8 June 2019; Accepted 14 June 2019
Available online 15 June 2019

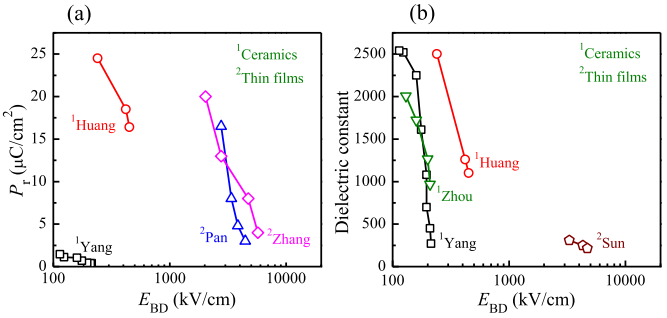

Fig. 1. Change in remanent polarization (P_r) and dielectric constant with breakdown strength. The data were obtained from Yang et al. [11], Sun et al. [14], Zhang et al. [16], Pan et al. [19], Zhou et al. [21] and Huang et al. [22].

the enhancement of breakdown strength and energy-storage density could be found in $Pb_{0.9}La_{0.1}(Zr_{0.52}Ti_{0.48})O_3$ (PLZT) thin films with a 'compacted' dense structure when compared to those in thin films with a columnar-grain structure [8]. The recent reports indicated that a higher energy-storage density is obtained in film capacitors with a multilayer heterostructure due to the larger E_{BD} value [14–18]. The superior breakdown strength in the multilayer heterostructure could be related to the formation of interfacial charge coupling between two different ferroelectric layers [14,15,18] or the formed built-in electric field at the heterointerface between ferroelectric and insulator layers [16]. In addition, it was also revealed that the transformation of ferroelectric macroscopic domains into polar nano-regions (PNRs) concurrently improved the breakdown strength and energy-storage density [19,20]. According to above reports, there are many ways to improve the breakdown strength of dielectric capacitors, but there are still some problems that relate to the main cause for enhanced breakdown strength properties. Based on the analysis of the properties in the above studies, we have found one common point in which the increase of breakdown strength was mainly ascribed to the decrement in dielectric constant and/or remanent polarization, as shown in Fig. 1.

In order to further clarify the relationship between the dielectric constant and/or remanent polarization and the breakdown strength, the properties of thin-film capacitors based on ferroelectric $Pb(Zr_{0.52}Ti_{0.48})O_3$ (PZT) and relaxor ferroelectric PLZT have been investigated. In this study, both films have similar deposition conditions, thicknesses, microstructures, crystalline orientation and crystalline quality. As a result, the PLZT thin films display outstanding comprehensive energy-storage performance (U_{reco} = 68.2 J/cm^3 and η = 80.4%) due to the slimmer *P-E* loop (or lower P_r) and large E_{BD} (3600 kV/cm) induced by the presence of PNRs in relaxor ferroelectrics. Furthermore, both the energy-storage performance and breakdown strength show excellent thermal stability in the relaxor PLZT thin films over a wide range of operating temperatures (25–200 °C). The relationship between remnant polarization/dielectric constant and breakdown strength is also discussed.

2. Experimental procedure

Pulsed laser deposition. Ferroelectric PZT and relaxor ferroelectric PLZT thin films were deposited on (001)$SrRuO_3$/$SrTiO_3$/Si substrates using pulsed laser deposition with a KrF excimer laser source (Lambda Physik, 248-nm wavelength). The 20-nm-thick epitaxial $SrTiO_3$ buffer layer was grown by reactive molecular-beam epitaxy on a Si substrate and acted as a seed layer for highly (001)-oriented epitaxial growth of the subsequent perovskite layers [23].

The optimized deposition conditions of the PZT and PLZT thin films were a laser repetition rate of 10 Hz, an energy density of 2.5 J/cm^2, an oxygen pressure of 0.1 mbar and a substrate temperature of 600 °C [24]. For the top and bottom $SrRuO_3$ electrodes, the conditions were a laser repetition rate of 4 Hz, an energy density of 2.5 J/cm^2, an oxygen pressure of 0.13 mbar and a substrate temperature of 600 °C. The thickness of the PZT and PLZT thin films was about 1 μm, while the thickness of the top and bottom $SrRuO_3$ electrodes was about 100 nm. In this study, the conductive-oxide $SrRuO_3$ electrodes were used to prevent the degradation of polarization and then the energy-storage properties [25].

Fabrication of thin-film capacitors. The capacitor structures (100 μm × 100 μm) were patterned with a standard photolithography process and structured by argon ion beam etching of the $SrRuO_3$ top electrodes and wet-chemical etching (HF–HCl solution) of the PZT and PLZT films.

Analysis and characterization. The crystallographic properties of the thin films were analyzed by X-ray diffraction (XRD) with θ-2θ scans using a PANalytical X-ray diffractometer (Malvern PANalytical) that used Cu-$K\alpha$ radiation with a wavelength of 1.5405 Å. The normal operating power was 1.8 kW (45 kV and 40 mA). Atomic force microscopy (AFM, Bruker Dimension Icon) and cross-sectional high-resolution scanning electron microscopy (SEM, Zeiss-1550, Carl Zeiss Microscopy GmbH) were performed to investigate the surface morphology, microstructure and thickness of the as-grown thin films.

The *P-E* hysteresis loops and switching current-electric field (I_S-*E*) curves were collected with dynamic hysteresis measurements in a ferroelectric module of the aixACCT TF-2000 Analyzer (aixACCT Systems GmbH). The capacitance-electric field (*C-E*) curves were measured using a slowly sweeping *dc*-electric field with on top a 1 kHz *ac*-voltage of 0.2 V. A Keithley 4200 semiconductor characterization system (Tektronix, Beaverton-Oregon, USA) was used for the leakage current measurement.

3. Results and discussion

The XRD patterns for the PZT and PLZT thin films are shown in Fig. 2a and b. The data indicate that the PZT and PLZT thin films on $SrTiO_3$/Si exhibited a (001) orientation. To further validate the crystalline quality of the thin films, the rocking curves for the (002) peaks in the PZT and PLZT thin films were measured (Fig. 2d). The full-width at half maximum values of the rocking curves for the (002) peaks are ~0.41° for both PZT and PLZT thin films, indicating a good crystalline quality for the thin films. The width of the rocking curve is a measure of the range over which the lattice structure in the different grains tilts with respect to the film normal [26] and is therefore an indication of the homogeneity of the thin films.

The surface morphology and grain growth of the thin films can be seen in Fig. 3. The results reveal that a very dense microstructure was observed in the PZT and PLZT thin films (Fig. 3a,c). The root-mean-square roughness (R_{rms}) values were calculated from the AFM images

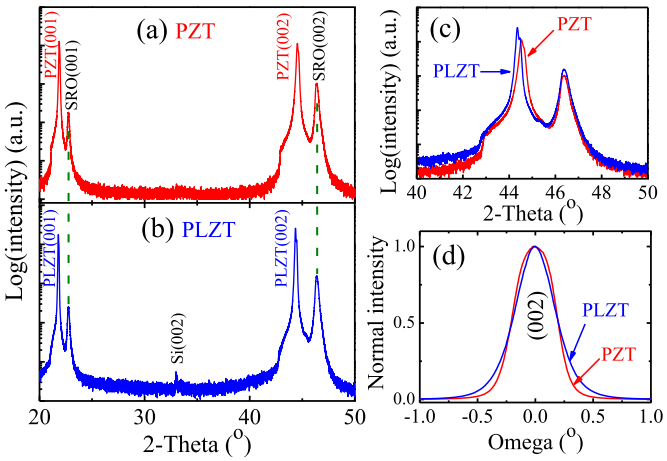

Fig. 2. XRD patterns for (a) PZT and (b) PLZT thin films. (c) Zoomed-in XRD patterns near (002) peaks and (d) rocking curves for the (002) peaks of these films.

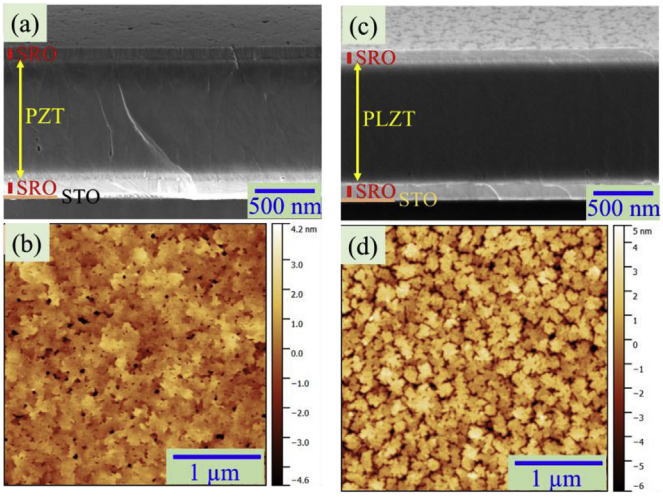

Fig. 3. Cross-sectional SEM and surface AFM images, respectively, for the (a,b) PZT and (c,d) PLZT thin films.

(Fig. 3b,d) and are ~0.9 and ~1.6 nm for the PZT and PLZT thin films, respectively. Combining of the results in Figs. 2 and 3 indicate that the crystalline quality and microstructure of PZT and PLZT in this study are similar.

A comparison of the *P-E* hysteresis loops at 500 kV/cm between the PZT and PLZT thin films is illustrated in Fig. 4a. The normal ferroelectric PZT thin films exhibit a strong ferrielectric property with a large maximum polarization (P_{max}) of 56.8 μC/cm^2 and a remanent polarization (P_r) of 32.5 μC/cm^2, and high coercive field (E_c) of 25.8 kV/cm. In the relaxor ferroelectric PLZT thin films, the P_{max} gradually reduces to 44.2 μC/cm^2, but a sharp decrease in P_r (0.66 μC/cm^2) and E_c (3.82 kV/cm) is observed. The good ferroelectric property in the PZT thin films can be also observed in the switching current curve in Fig. 4b, where the sharp switching peaks with a high intensity are obtained. Meanwhile, the four switching peaks in the switching current curve are detected in the relaxor PLZT films and indicated its antiferroelectric-like behavior [27]. As explained previously, the minimized P_r and E_c values are due to the presence of PNRs in the relaxor PLZT, which was decomposed from the macroscopic ferroelectric domains in the normal ferroelectric PZT. Fig. 5 shows the unit cells of undoped PZT and PLZT perovskite materials. As a donor dopant, La doping in PZT leads to the generation of excess electrons that tend to suppress oxygen vacancy ($\ddot{V}_O$) formation according to the following equations:

$$Pb \xrightarrow{2La} 2La_{\dot{P}b} + V'_{Pb} + 2e \quad (4)$$

$$\ddot{V}_O + 2e \rightarrow null \quad (5)$$

Moreover, the substitution of La^{3+} for Pb^{2+} ions necessarily leads to the formation of lead vacancies (V'_{Pb}) at the A sites in order to

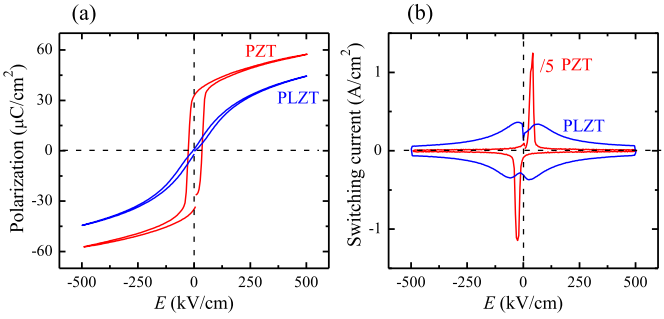

Fig. 4. (a) *P-E* hysteresis loops and (b) switching current of PZT and PLZT thin films measured at 500 kV/cm.

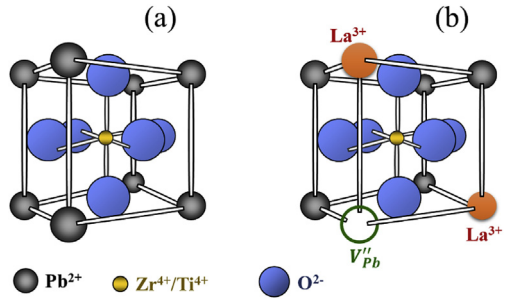

Fig. 5. Schematic diagrams of (a) undoped PZT unit cell and (b) PLZT unit cell with substitutional doping of La^{3+} at the Pb^{2+} sites.

maintain the charge neutrality in the PLZT unit cell [28–30] (charge imbalance is created that must be compensated by ionic compensation as cation V'_{Pb} vacancies, as shown in Fig. 5b). The presence of $La_{\dot{P}b}$ defects near the V'_{Pb} vacancies leads to immobile ($V'_{Pb} - La_{\dot{P}b}$) dipolar defects within the PLZT unit cell [28]. The existence of the local disorder in the distribution of the cations creates a quenched random local field. This field breaks the long-range ordered ferroelectric (macroscopic) domains (Fig. 6a) in ferroelectrics into the smaller PNRs (Fig. 6b) that appear in relaxor ferroelectrics [21,31]. All the domains are aligned along the direction of the applied electric field ($E \rightarrow E_{max}$). When the applied electric field is removed ($E \rightarrow 0$), the normal ferroelectrics present a high P_r value induced by a slowly back-switching of macroscopic domains, whereas the PNRs in the relaxor ferroelectrics are more easily returned to their random orientations due to the much smaller size of PNRs, and therefore lead to slim polarization hysteresis loops along with low P_r and E_c values.

As discussed above, in order to obtain a high energy-storage density, a large applied electric field needs to be used. Fig. 7 shows the *P-E* hysteresis loops of PZT and PLZT thin films, measured from a low electric field up to their corresponding E_{BD}. The E_{BD} values are ~1000 and ~3600 kV/cm, respectively, for normal ferroelectric PZT and relaxor ferroelectric PLZT thin films. Similar to the previous studies, as indicated in Fig. 1, the enhancement of maximum applied electric field (E_{BD}) for the PLZT thin film is also mainly ascribed to the decrement in dielectric constant (Fig. 8a) and remanent polarization (Fig. 9c). Moreover, the lower leakage current density observed in the PLZT thin film (Fig. 8b) is due to the reduction of oxygen vacancies that can

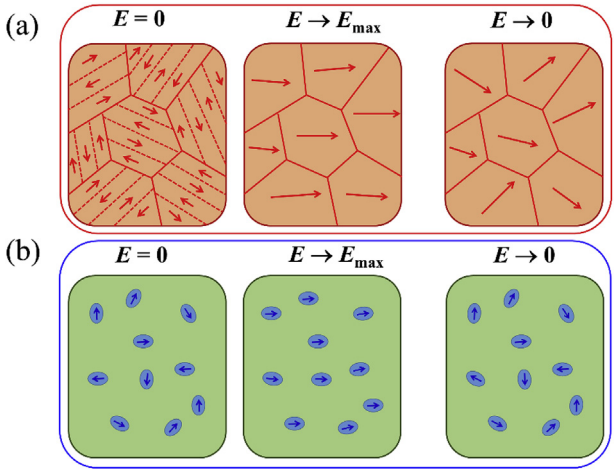

Fig. 6. Schematic diagrams of domain structure at initial stage in (a) a normal ferroelectric, where the solid and dotted lines represent the grain boundaries and ferroelectric domain walls, respectively, and (b) a relaxor ferroelectric, where the PNRs are represented by the ellipse. ($E \rightarrow E_{max}$): domains are aligned in the direction of the applied electric field; ($E \rightarrow 0$): domain configurations in ferroelectric and relaxed ferroelectric after removing the electric field.

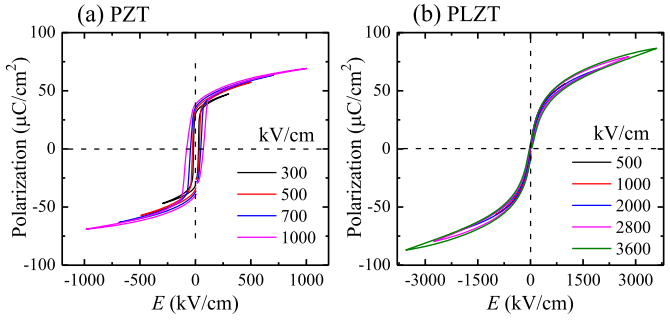

Fig. 7. *P-E* hysteresis loops of (a) PZT and (b) PLZT thin films, measured at various electric fields.

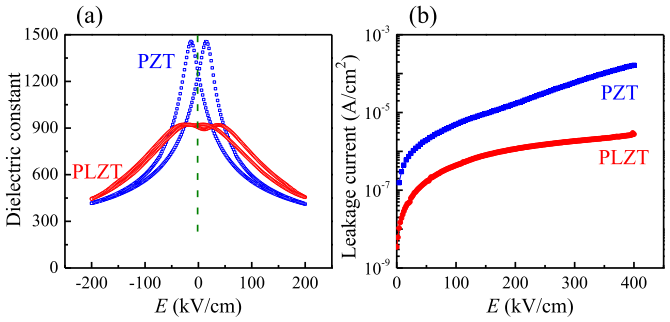

Fig. 8. (a) Dielectric constant and (b) leakage current density of PZT and PLZT thin films. The dielectric constants defined at 0 kV/cm are ~1260 and ~910, and the leakage currents at 400 kV/cm are 1.66×10^{-4} and 2.66×10^{-6} J/cm^2, respectively, for PZT and PLZT films.

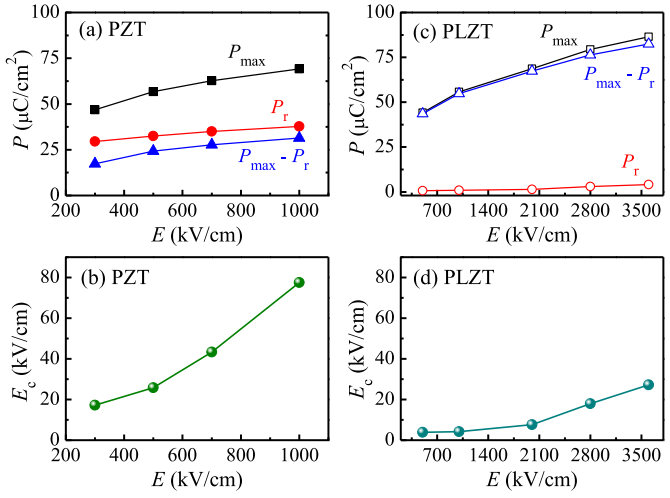

Fig. 9. P_{max}, P_r, $P_{max} - P_r$ and E_c of (a,b) PZT and (c,d) PLZT thin films as a function of electric field.

prevent the percolating pathway of conduction, and then the E_{BD} value is enhanced [11,32,33].

As shown in Fig. 9a and b, the P_{max} increases gradually whereas the P_r increases slightly with increasing applied electric field. Therefore, the ($P_{max} - P_r$) increases gradually upon increasing electric field. The significant enhancement of the P_{max} and ($P_{max} - P_r$) values would certainly be beneficial to improving the energy-storage density that will be discussed in detail in the following sections. Fig. 9c and d shows the value of coercive field (E_c) for PZT and PLZT thin films with different electric fields. It can be found that E_c shows an increment trend with increasing electric field; however, the PLZT thin film has a much slimmer *P-E* loop due to the much lower E_c value measured at the same electric field. The E_c values of the PZT and PLZT thin films, measured at

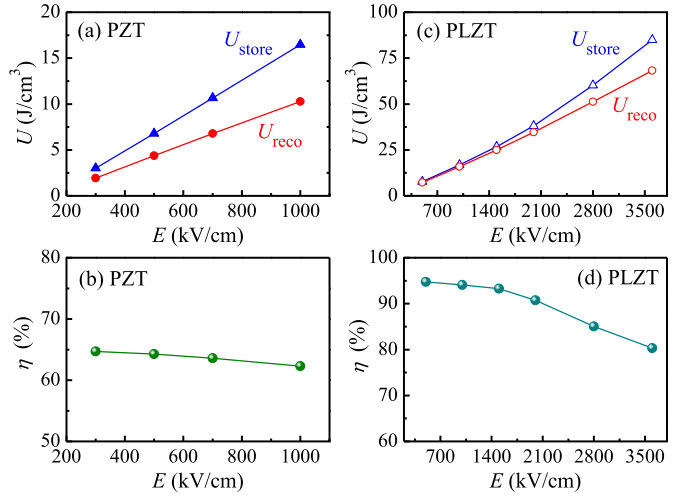

Fig. 10. Dependence of energy-storage density (U_{store} and U_{reco}) and energy-storage efficiency (η) on applied electric field for (a,b) PZT and (c,d) PLZT thin films. The data were calculated from the corresponding *P-E* hysteresis loops, as indicated in Fig. 7.

an applied electric field of 1000 kV/cm, are 77.5 and 4.1 kV/cm, respectively.

The effect of applied electric field on the energy-storage properties of thin-film capacitors was investigated in detail and is shown in Fig. 10. As expected, both the energy stored per unit volume (U_{store}) and recoverable energy-storage density (U_{reco}) values increase with a larger electric field. At 1000 kV/cm, the U_{store} and U_{reco} are 16.5 and 10.3 J/cm^3, and 16.9 and 15.9 J/cm^3, respectively, for the PZT and PLZT thin films. Similar to the difference between the P_{max} and ($P_{max} - P_r$) values, the change in the U_{store} and U_{reco} is also observed with increasing electric field. However, the values of U_{reco} are closer to those of U_{store}, measured at the same electric field, observed in the PLZT thin films due to the slimmer *P-E* loops and the slow increase of the reduced P_r value. Therefore, although the energy-storage efficiency (η) in PLZT thin films slightly decreases as the electric field increases, it still maintains over 91% at the electric field up to 2000 kV/cm, and down to 80.4% at the E_{BD} of 3600 kV/cm. In practical applications, the energy efficiency is extremely important because higher energy efficiency ensures less energy dissipation (energy loss) during charging and discharging, which can enhance the discharge speed. Due to the large E_{BD}, the PLZT thin films exhibit an ultrahigh U_{reco} of 68.2 J/cm^3 while maintaining a high efficiency, which makes them a promising candidate for high energy-storage applications.

The thermal stability of dielectric capacitors is essential for effective thermal management in power energy systems. Depending on the application and operating environmental conditions, the capacitors may be subjected to a wide range of temperatures from −90 to 250 °C [34–36]. The effect of measured (operating) temperature on the energy storage and energy efficiency have been mentioned in many reports, in which both U_{reco} and η values were almost decreased with the increment of operating temperature [12,14,19,25,27]. However, the effect of operating temperature on the electric breakdown strength still has not received much attention. The thermal stability of the energy-storage performances for the PZT and PLZT thin films was investigated under an electric field of 500 kV/cm and in the temperature range from room temperature to 200 °C. A slight broadening tendency of *P-E* loops and reduced P_{max} values are observed with increasing temperature, as given in Fig. 11a and b, which signify its weak degradation of energy density and efficiency. As shown in Fig. 11c and d, the fluctuations in U_{reco} and η are about −10% and −18% for the PZT thin film, respectively, and less than −6% for the PLZT thin film over the above temperature range. The excellent thermal stability of the PLZT thin film is probably related

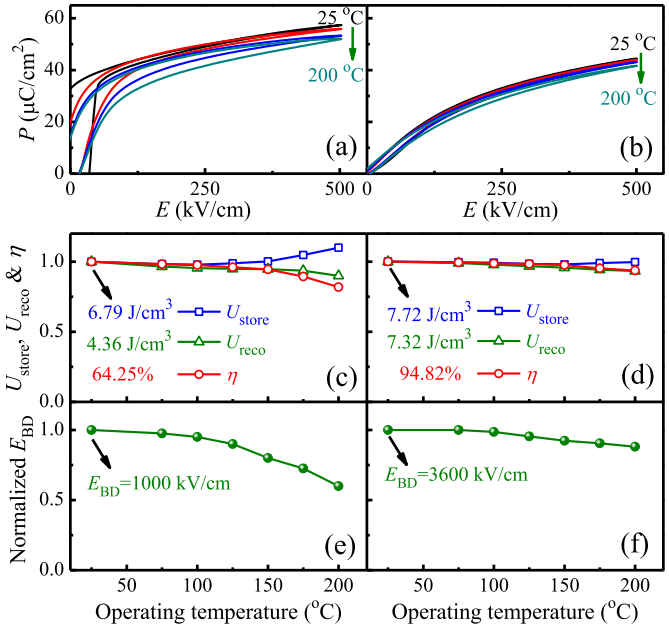

Fig. 11. Measured temperature dependence of (a,b) *P-E* loops, (c,d) energy storage and efficiency, and (e,f) breakdown strength, respectively, for PZT and PLZT thin films. The measurements were performed at 500 kV/cm and 1 kHz.

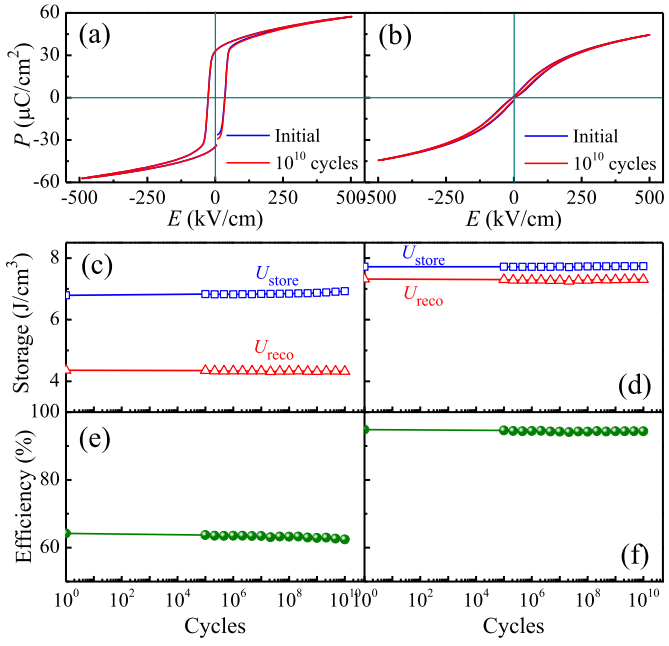

Fig. 12. Dependence of charge-discharge cycle on (a,b) *P-E* loops, (c,d) energy storage and (e,f) energy efficiency, respectively, for PZT and PLZT thin films. The measurements were performed at 500 kV/cm, 1 kHz and room temperature.

to the relaxor behavior with the presence of PNRs [21,37,38]. Moreover, the presence of PNRs in the relaxor PLZT thin film can also be observed from the relationship between operating temperature and breakdown strength of thin-film capacitors. It can be seen from Fig. 11e and f that the E_{BD} of the PLZT thin film gradually decreases with increasing operating temperature (−12%, from 3600 to 3175 kV/cm), whereas the E_{BD} of the PZT thin film significantly reduces (−40%, from 1000 to 600 kV/cm). The excellent E_{BD} at high operating temperatures combined with the excellent temperature stability of energy storage and efficiency indicate that the PLZT thin film has significant potential in widespread applications in energy-storage applications and in various working environments.

Long-term working stability is another significant requirement for the application of energy storage capacitors. Fig. 12a and b shows the *P-E* hysteresis loops of PZT and PLZT thin films with respect to various charge-discharge cycles (until 10^{10} cycles) measured at 500 kV/cm, 1 kHz and room temperature. These results indicate that there are no significant change in the *P-E* loops, resulting in the fatigue-free behavior in both energy storage and energy efficiency of thin film capacitors during electric field cycling, as shown in Fig. 12c–f. The fatigue-free behavior of the thin film capacitors in this study is likely due to the inhibition of the accumulation of oxygen vacancies near the film/electrode interfaces during the charge-discharging cycling process by using conductive metallic-oxide SrRuO3 layers as the top- and bottom-electrodes [25,39].

4. Conclusions

In summary, an ultrahigh U_{reco} of 68.2 J/cm^3 with a large energy efficiency of 80.4% has been achieved in the relaxor ferroelectric PLZT thin films. The slim polarization hysteresis (*P-E*) loops of PLZT thin films demonstrate a negligible P_r and high (P_{max} – P_r) due to the presence of polar nano-regions (PNRs). Interestingly, the dielectric constant and remanent polarization seem to effect the breakdown strength, in which PNR-induced very small remanent polarization and low dielectric constant results in excellent E_{BD} and ultrahigh U_{reco} values in the PLZT thin films. Moreover, the relaxor PLZT thin films exhibit superior charge-discharge cycling performance and excellent thermal stability in not only energy density and efficiency, but also breakdown strength. All of these results indicate that the relaxor PLZT thin-film capacitors are suitable for the pulse-driving energy-storage applications in various working environments.

Conflicts of interest

The authors declare no conflict of interest.

Acknowledgements

The authors would like to acknowledge the financial support from the National Foundation for Science and Technology Development of Vietnam under Grant No. 103.99-2018.23.

References

[1] B. Chu, X. Zhou, K. Ren, B. Neese, M. Lin, Q. Wang, F. Bauer, Q.M. Zhang, A dielectric polymer with high electric energy density and fast discharge speed, Science 313 (5785) (2006) 334–336.
[2] I. Husain, Electric and Hybrid Vehicles: Design Fundamentals, second ed., CRC Press, Boca Raton, FL, 2010.
[3] H. Bluhm, D. Rusch, Pulsed Power Systems: Principles and Applications, Springer, Berlin, 2006.
[4] P. Khanchaitit, K. Han, M.R. Gadinski, Q. Li, Q. Wang, Ferroelectric polymer networks with high energy density and improved discharged efficiency for dielectric energy storage, Nat. Commun. 4 (2013) 2845.
[5] O. Ohm, D. Danilovic, Improvements in pacemaker energy consumption and functional capability: four decades of progress, Pacing Clin. Electrophysiol. 20 (1) (1997) 2–9.
[6] M. Farhadi, O. Mohammed, Energy storage technologies for high-power applications, IEEE Trans. Ind. Appl. 52 (3) (2016) 1953–1961.
[7] X. Hao, A review on the dielectric materials for high energy-storage application, J. Adv. Dielectr. 03 (01) (2013) 1330001.
[8] M.D. Nguyen, E.P. Houwman, G. Rijnders, Energy storage performance and electric breakdown field of thin relaxor ferroelectric PLZT films using microstructure and growth orientation control, J. Phys. Chem. C 122 (27) (2018) 15171–15179.
[9] H. Yang, F. Yan, Y. Lin, T. Wang, Novel strontium titanate-based lead-free ceramics for high-energy storage applications, ACS Sustain. Chem. Eng. 5 (11) (2017) 10215–10222.
[10] T. Wang, L. Jin, C. Li, Q. Hu, X. Wei, Relaxor ferroelectric $BaTiO_3$–$Bi(Mg_{2/3}Nb_{1/3})O_3$ ceramics for energy storage application, J. Am. Ceram. Soc. 98 (2) (2015) 559–566.
[11] H. Yang, F. Yan, Y. Lin, T. Wang, L. He, F. Wang, A lead free relaxation and high

energy storage efficiency ceramics for energy storage applications, J. Alloy. Comp. 710 (2017) 436–445.
[12] Y. Zhao, X. Hao, Q. Zhang, Energy-storage properties and electrocaloric effect of $Pb_{(1-3x/2)}La_xZr_{0.85}Ti_{0.15}O_3$ antiferroelectric thick films, ACS Appl. Mater. Interfaces 6 (14) (2014) 11633–11639.
[13] M. Rahimabady, S. Chen, K. Yao, F.E.H. Tay, L. Lu, High electric breakdown strength and energy density in vinylidene fluoride oligomer/poly(vinylidene fluoride) blend thin films, Appl. Phys. Lett. 99 (14) (2011) 142901.
[14] Z. Sun, C. Ma, M. Liu, J. Cui, L. Lu, J. Lu, X. Lou, L. Jin, H. Wang, C.L. Jia, Ultrahigh energy storage performance of lead-free oxide multilayer film capacitors via interface engineering, Adv. Mater. 29 (5) (2017) 1604427.
[15] H. Pan, Q. Zhang, M. Wang, S. Lan, F. Meng, J. Ma, L. Gu, Y. Shen, P. Yu, Y.H. Lin, C.W. Nan, Enhancements of dielectric and energy storage performances in lead-free films with sandwich architecture, J. Am. Ceram. Soc. 102 (3) (2019) 936–943.
[16] T. Zhang, W. Li, Y. Zhao, Y. Yu, W. Fei, High energy storage performance of opposite double-heterojunction ferroelectricity–insulators, Adv. Funct. Mater. 28 (10) (2018) 1706211.
[17] S. Cho, C. Yun, Y.S. Kim, H. Wang, J. Jian, W. Zhang, J. Huang, X. Wang, H. Wang, J.L. MacManus-Driscoll, Strongly enhanced dielectric and energy storage properties in lead-free perovskite titanate thin films by alloying, Nano Energy 45 (2018) 398–406.
[18] H. Zhu, M. Liu, Y. Zhang, Z. YZ, J. Ouyang, W. Pan, Increasing energy storage capabilities of space-charge dominated ferroelectric thin films using interlayer coupling, Acta Mater. 122 (2017) 252–258.
[19] H. Pan, J. Ma, J. Ma, Q. Zhang, X. Liu, B. Guan, L. Gu, X. Zhang, Y.J. Zhang, L. Li, Y. Shen, Y.H. Lin, C.W. Nan, Giant energy density and high efficiency achieved in bismuth ferrite-based film capacitors via domain engineering, Nat. Commun. 9 (1) (2018) 1813.
[20] B. Peng, Q. Zhang, X. Li, T. Sun, H. Fan, S. Ke, M. Ye, Y. Wang, W. Lu, H. Niu, J.F. Scott, X. Zeng, H. Huang, Giant electric energy density in epitaxial lead-free thin films with coexistence of ferroelectrics and antiferroelectrics, Adv. Electron. Mater. 1 (5) (2015) 1500052.
[21] M. Zhou, R. Liang, Z. Zhou, X. Dong, Combining high energy efficiency and fast charge-discharge capability in novel $BaTiO_3$-based relaxor ferroelectric ceramic for energy-storage, Ceram. Int. 45 (3) (2019) 3582–3590.
[22] W. Huang, Y. Chen, X. Li, G. Wang, N. Liu, S. Li, M. Zhou, X. Dong, Ultrahigh recoverable energy storage density and efficiency in barium strontium titanate-based lead-free relaxor ferroelectric ceramics, Appl. Phys. Lett. 113 (20) (2018) 203902.
[23] C. Marchiori, M. Sousa, A. Guiller, H. Siegwart, J.P. Locquet, J. Fompeyrine, G.J. Norga, J.W. Seo, Thermal stability of the $SrTiO_3$/(Ba,Sr)O stacks epitaxially grown on Si, Appl. Phys. Lett. 88 (7) (2006) 072913.
[24] M.D. Nguyen, E. Houwman, M. Dekkers, H.N. Vu, G. Rijnders, A fast room-temperature poling process of piezoelectric $Pb(Zr_{0.45}Ti_{0.55})O_3$ thin films, Sci. Adv. Mater. 6 (2) (2014) 243–251.
[25] M.D. Nguyen, C.T.Q. Nguyen, H.N. Vu, G. Rijnders, Controlling microstructure and film growth of relaxor-ferroelectric thin films for high break-down strength and energy-storage performance, J. Eur. Ceram. Soc. 38 (1) (2018) 95–103.
[26] E.P. Houwman, M.D. Nguyen, M. Dekkers, G. Rijnders, Intrinsic stability of ferroelectric and piezoelectric properties of epitaxial $PbZr_{0.45}Ti_{0.55}O_3$ thin films on silicon in relation to grain tilt, Sci. Technol. Adv. Mater. 14 (4) (2013) 045006.
[27] M.D. Nguyen, G. Rijnders, Electric field-induced phase transition and energy storage performance of highly-textured $PbZrO_3$ antiferroelectric films with a deposition temperature dependence, J. Eur. Ceram. Soc. 38 (15) (2018) 4953–4961.
[28] D. Mukherjee, M. Hordagoda, D. Pesquera, D. Ghosh, J.L. Jones, P. Mukherjee, S. Witanachchi, Enhanced ferroelectric polarization in epitaxial $(Pb_{1-x}La_x)(Zr_{0.52}Ti_{0.48})O_3$ thin films due to low La doping, Phys. Rev. B 95 (17) (2017) 174304.
[29] W. Zhu, I. Fujii, W. Ren, S. Trolier-McKinstry, Domain wall motion in A and B site donor-doped $Pb(Zr_{0.52}Ti_{0.48})O_3$ films, J. Am. Ceram. Soc. 95 (9) (2012) 2906–2913.
[30] S.K. Ghosh, M. Ganguly, S.K. Rout, T.P. Sinha, Order-disorder correlation on local structure and photo-electrical properties of La^{3+} ion modified BZT ceramics, Eur. Phys. J. Plus 130 (4) (2015) 68.
[31] J. Wu, A. Mahajan, L. Riekehr, H. Zhang, B. Yang, N. Meng, Z. Zhang, H. Yan, Perovskite $Sr_x(Bi_{1-x}Na_{0.97-x}Li_{0.03})_{0.5}TiO_3$ ceramics with polar nano regions for high power energy storage, Nano Energy 50 (2018) 723–732.
[32] C. Reitz, P.M. Leufke, H. Hahn, T. Brezesinski, Ordered mesoporous thin film ferroelectrics of biaxially textured lead zirconate titanate (PZT) by chemical solution deposition, Chem. Mater. 26 (6) (2014) 2195–2202.
[33] Y. Wu, X. Wang, C. Zhong, L. Li, Effect of anneal conditions on electrical properties of Mn-doped $(Na_{0.85}K_{0.15})_{0.5}Bi_{0.5}TiO_3$ thin films prepared by sol–gel method, J. Am. Ceram. Soc. 94 (6) (2011) 1843–1849.
[34] H. Palneedi, M. Peddigari, G.T. Hwang, D.Y. Jeong, J. Ryu, High-performance dielectric ceramic films for energy storage capacitors: progress and outlook, Adv. Funct. Mater. 28 (42) (2018) 1803665.
[35] B. Fan, F. Liu, G. Yang, H. Li, G. Zhang, S. Jiang, W. Wang, Dielectric materials for high-temperature capacitors, IET Nanodielectr 1 (1) (2018) 32–40.
[36] X. Lin, M. Salari, L.M.R. Arava, P.M. Ajayan, M.W. Grinstaff, High temperature electrical energy storage: advances, challenges, and frontiers, Chem. Soc. Rev. 45 (21) (2016) 5848–5887.
[37] J. Shi, X. Liu, W. Tian, High energy-storage properties of $Bi_{0.5}Na_{0.5}TiO_3$-$BaTiO_3$-$SrTi_{0.875}Nb_{0.1}O_3$ lead-free relaxor ferroelectrics, J. Mater. Sci. Technol. 34 (12) (2018) 2371–2374.
[38] F. Li, M. Zhou, J. Zhai, B. Shen, H. Zeng, Novel barium titanate based ferroelectric relaxor ceramics with superior charge-discharge performance, J. Eur. Ceram. Soc. 38 (14) (2018) 4646–4652.
[39] M.D. Nguyen, H. Yuan, E.P. Houwman, M. Dekkers, G. Koster, J.E. ten Elshof, G. Rijnders, Highly oriented growth of piezoelectric thin films on silicon using two-dimensional nanosheets as growth template layer, ACS Appl. Mater. Interfaces 8 (45) (2016) 31120–31127.